Eur Radiol (2016) 26:3102–3111
DOI 10.1007/s00330-015-4136-y

HEPATOBILIARY-PANCREAS

Identification of Imaging Predictors Discriminating Different Primary Liver Tumours in Patients with Chronic Liver Disease on Gadoxetic Acid-enhanced MRI: a Classification Tree Analysis

Hyun Jeong Park[1] · Kyung Mi Jang[2] · Tae Wook Kang[2] · Kyoung Doo Song[2] · Seong Hyun Kim[2] · Young Kon Kim[2] · Dong Ik Cha[2] · Joungyoun Kim[3] · Juna Goo[3]

Received: 21 June 2015 / Revised: 8 November 2015 / Accepted: 23 November 2015 / Published online: 3 December 2015

Abstract

Objectives To identify predictors for the discrimination of intrahepatic cholangiocarcinoma (IMCC) and combined hepatocellular-cholangiocarcinoma (CHC) from hepatocellular carcinoma (HCC) for primary liver cancers on gadoxetic acid-enhanced MRI among high-risk chronic liver disease (CLD) patients using classification tree analysis (CTA).

Methods A total of 152 patients with histopathologically proven IMCC ($n = 40$), CHC ($n = 24$) and HCC ($n = 91$) were enrolled. Tumour marker and MRI variables including morphologic features, signal intensity, and enhancement pattern were used to identify tumours suspicious for IMCC and CHC using CTA.

Results On CTA, arterial rim enhancement (ARE) was the initial splitting predictor for assessing the probability of tumours being IMCC or CHC. Of 43 tumours that were classified in a subgroup on CTA based on the presence of ARE, non-intralesional fat, and non-globular shape, 41 (95.3 %) were IMCCs ($n = 29$) or CHCs ($n = 12$). All 24 tumours showing fat on MRI were HCCs. The CTA model demonstrated sensitivity of 84.4 %, specificity of 97.8 %, and accuracy of 92.3 % for discriminating IMCCs and CHCs from HCCs.

Conclusions We established a simple CTA model for classifying a high-risk group of CLD patients with IMCC and CHC. This model may be useful for guiding diagnosis for primary liver cancers in patients with CLD.

Key Points

- *Arterial rim enhancement was the initial splitting predictor on CTA.*
- *CTA model achieved high sensitivity, specificity, and accuracy for discrimination of tumours.*
- *This model may be useful for guiding diagnosis of primary liver cancers.*

Keywords Hepatocellular carcinoma · Cholangiocarcinoma · Combined hepatocellular-cholangiocarcinoma · Gadoxetic acid · Classification tree analysis

Introduction

Hepatocellular carcinoma (HCC) is the most common primary liver cancer in patients with chronic liver disease (CLD), and is typically thought to be caused by viral infection (hepatitis B or C) and alcoholism. However, such patients are also at significantly increased risk of intrahepatic mass-forming cholangiocarcinoma (IMCC) [1–3]. In addition, combined hepatocellular-cholangiocarcinoma (CHC) has many demographic and clinical similarities to IMCC, and also shares etiological risk factors with HCC [4, 5]. Various therapeutic methods, including liver transplantation, surgical resection, radiofrequency ablation (RFA), and transarterial chemoembolization (TACE), can be applied for the treatment of HCC [6]. However, for IMCC and CHC, surgical resection

✉ Kyung Mi Jang
kmmks.jang@samsung.com

[1] Department of Radiology, Chung-Ang University Hospital, Chung-Ang University College of Medicine, 102 Heukseok-ro, Dongjak-gu, Seoul 156-755, Republic of Korea

[2] Department of Radiology and Center for Imaging Science, Samsung Medical Center, Sungkyunkwan University School of Medicine, Seoul, Republic of Korea

[3] Biostatistics and Clinical Epidemiology Center, Samsung Medical Center, Sungkyunkwan University School of Medicine, Seoul, Republic of Korea

is the most effective and is the only therapy associated with prolonged disease-free survival, whereas liver transplantation is generally contraindicated because of the high rate of recurrence [7–11].

Advances in MR imaging technology and the development of tissue-specific contrast material such as gadoxetic acid have made it possible to differentiate most HCCs from IMCCs and CHCs based on their typical signal intensities and enhancement patterns [12–19]. A diagnosis of HCC is currently based primarily on imaging findings according to the guidelines established by the American Association for the Study of Liver Diseases (AASLD) [6]. However, HCCs can show atypical enhancement patterns on gadoxetic acid-enhanced MR imaging [17, 20, 21], and small IMCCs can show arterial hypervascularity with delayed washout similar to that in HCC [18, 19]. In addition, imaging features of CHC may overlap with those of classic HCC or IMCC [10, 18, 22]. Although percutaneous liver biopsy prior to treatment is typically considered for differentiation of IMCC and CHC from HCC, seeding to the peritoneum or along the needle tract has occasionally been reported [23, 24]. Therefore, in high-risk CLD patients, it is important to identify predictors for discriminating IMCC and CHC from HCC in primary liver cancer using gadoxetic acid-enhanced MRI.

For this purpose, we employ classification tree analysis (CTA). CTA is a machine-learning method of predicting the class levels (e.g., IMCC and CHC) of an outcome variable based on several predictors. The advantages of CTA include (1) its robustness to normalization, scaling, and outliers of data, (2) the lack of a need for linearity assumptions in the data, and (3) its ability to visually and explicitly represent the prediction process [25].

Accordingly, the purpose of this study was to identify the predictors for the discrimination of IMCC and CHC from HCC for primary liver cancers on gadoxetic acid-enhanced MRI among a group of high-risk CLD patients through the use of CTA.

Materials and methods

Study population

This retrospective study was approved by our institutional review board, and the requirement for informed consent was waived. Using our institutional surgical pathologic data, we retrospectively searched cases of IMCC and CHC between January 2012 and January 2015, and HCC between January 2014 and January 2015. Those meeting the following inclusion criteria were then selected for this study: (a) patients who met the Milan criteria [26], (b) who were diagnosed with chronic liver disease according to pathologic or clinical criteria [27], (c) who had no history of previous treatment for hepatic tumour, and (d) who underwent gadoxetic acid-enhanced liver MR imaging according to our standard protocol within 1 month prior to surgery (Fig. 1). The median length of time between MR imaging and surgery was 17 days (range, 2–26 days). A total of 152 patients with 155 tumours were included in this study. Among these, 64 patients with 40 IMCCs and 24 CHCs were defined as the cholangio-combined group, and 90 patients with 91 HCCs were defined as the HCC group. Three patients had two tumours each (two HCCs, one IMCC and one HCC, and one CHC and one HCC). The clinical and demographic data of the study groups are summarized on Table 1.

The preoperative serum levels of α-fetoprotein (AFP) and protein induced by vitamin K absence or antagonist-II (PIVKA-II) within 1 month prior to surgery were recorded.

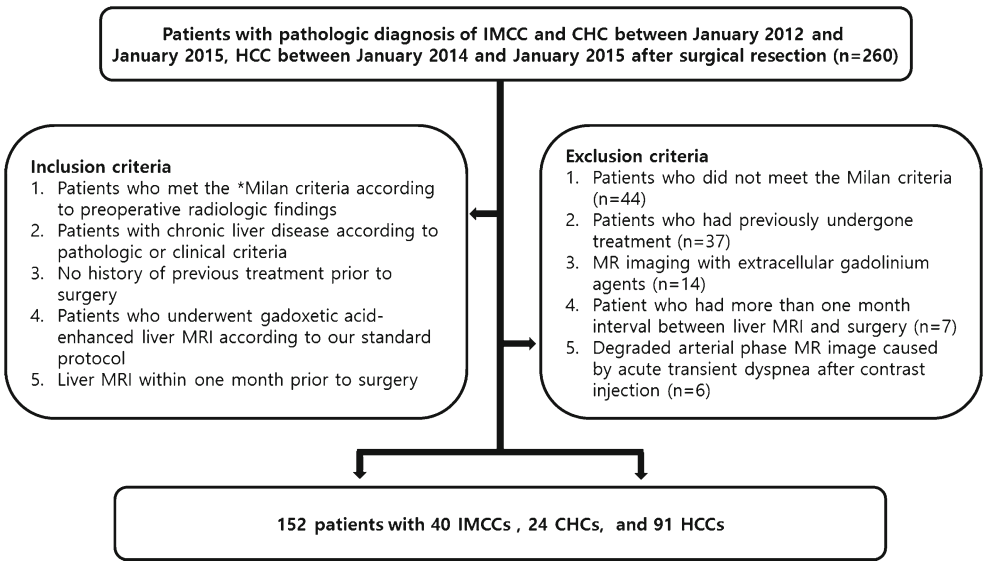

Fig. 1 Flowchart of the inclusion process for the study group. *IMCC* intrahepatic mass-forming cholangiocarcinoma, *CHC* combined hepatocellular-cholangiocarcinoma, *HCC* hepatocellular carcinoma. *Milan criteria = a solitary tumour with a diameter less than 5 cm, or up to three hepatic nodules, each smaller than 3 cm, with no evidence of vascular invasion or extrahepatic metastasis according to preoperative radiologic findings

Table 1 Clinical and demographic data

Characteristics	Cholangio-combined group	HCC group
No. of patients	64	90
Male/female	47/17	81/9
Mean age (years)	61.4	60.7
Age range (years)	32–78	31–82
AFP level (ng/mL)*		
Mean	9.46	490.8
Range	1.3–153.0	1.3–10569.0
PIVKA-II (mAU/mL)*		
Mean	28.08	759.3
Range	2.3–140.0	2.4–35940.0
Aetiology of liver disease (no. of patients)		
HBV	54	69
HCV	4	10
Alcoholic	5	4
NBNC	1	7
Chronic hepatitis (no. of patients)	46	50
Liver cirrhosis (no. of patients)	18	40
Pathology (no. of tumours)	64	91
IMCC	40	NA
CHC-HCC predominant	16	NA
CHC-CC predominant	8	NA
Edmondson–Steiner's classification		
I/II/III/IV	NA	4/76/10/1[†]
Tumour size (cm)		
Mean	3.3	2.9
Range	1.5–4.9	1.0–4.9

IMCC intrahepatic mass-forming cholangiocarcinoma originated from the epithelium of intrahepatic bile duct peripheral to the second order branch and morphologically mass-forming type with central fibrotic areas, *CHC* combined hepatocellular cholangiocarcinoma classified as transitional type according to Goodman's pathologic classification, *HCC* hepatocellular carcinoma, *CC* cholangiocarcinoma. *NA* not applicable. *HBV* hepatitis B virus, *HCV* hepatitis C virus, *NBNC* non-B, non-C. *Statistically significant difference between the two groups ($P > 0.0001$). [†] Five lesions were proven to be scirrhous HCC

At our institution, elevated AFP and PIVKA-II levels are defined as serum levels higher than 8.1 ng/mL and 40 mAU/mL, respectively. To determine patient eligibility for enrolment for this study, a review of pathologic reports, clinical data, and MR images was performed by one abdominal radiologist (H.J. P., with 9 years of experience in abdominal MRI interpretation).

Image acquisition

A 3-T whole-body MRI system (Intera Achieva 3.0 T; Philips Healthcare, Best, Netherlands) with a 32-channel phased-array (Torso/Cardiac, Philips Healthcare) receiver coil was used in this study. Liver images for all patients were acquired in the axial plane both before and after administration of gadoxetic acid at a dose of 0.1 mL/kg (0.025 mmol/kg). The contrast agent was administered intravenously at a rate of 2 mL/s using a power injector, followed by a 20-mL saline flush. The MRI protocol is summarized in Table 2. Diffusion-weighted imaging (DWI) was performed before the administration of gadoxetic acid using a respiratory-triggered single-shot echo planar imaging with b-values of 0, 100, and 800 s/mm^2. A spectral attenuated inversion recovery technique was used for fat suppression on DWI. The apparent diffusion coefficient was calculated using a monoexponential function with b values of 100 and 800 s/mm^2 in order to minimize perfusion effects. For gadoxetic acid-enhanced MRI, unenhanced, enhanced arterial phase (20–35 s), portal phase (60 s), 3-min delayed phase, and 10-min and 20-min delayed hepatobiliary phase images (HBPI) were obtained using a T1-weighted 3D turbo field-echo sequence (THRIVE [T1 high-resolution isotropic volume examination]; Philips Healthcare) with spectral attenuated inversion recovery fat suppression. The timing for the arterial phase imaging was determined using MR fluoroscopic bolus detection.

Table 2 MRI sequences and parameters

Sequence	TR/TE (ms)	FA	Section thickness (mm)	Matrix size	Bandwidth (Hz/ pixel)	Field of view (cm)	Acquisition time	No. of excitations
T1W- 2D dual GRE	3.5/1.15–2.3	10°	6	256 × 194	434.4	32–38	14	1
BH-MS-T2WI*	1623/70	90°	5	324 × 235	235.2	32–38	55/13.7	1
RT-SS-T2WI*	1342/80	90	5	320 × 256	506.4	32–38	120	2
RT-SS-HT2WI*	1156/160	90°	5	320 × 256	317.9	32–38	120	2
DWI	1600/70	90°	5	112 × 108	79.5	34	126	4
T1W-3D GRE	3.1/1.5	10°	2	256 × 256	995.7	32–38	16.6	1

FA flip angle, *GRE* gradient echo, *BH-MS-T2WI* breath-hold multi-shot T2-weighted image, *RT-SS-HT2WI* respiration-triggered single-shot heavily T2-weighted image. *Fat saturation images

Image analysis

All MR images were retrospectively and independently reviewed on a commercial workstation with a 2,000 × 2,000 PACS monitor (Centricity; GE Healthcare) by two abdominal radiologists (T.W.K. and K.D.S., with 10 and 7 years of experience in abdominal MRI interpretation, respectively) in a blinded manner. These reviewers were unaware of the pathological tumour diagnoses. In cases of disagreement, a third observer (S.H.K., with 16 years of experience in abdominal MRI) was asked for an opinion, and a majority decision was reached which was used for data analysis.

The MR imaging features that had been evaluated for investigation of IMCC, CHC, and HCC in previous studies [4, 9, 11, 13, 14, 16–19, 28, 29] are summarized in Table 3 (Figs. 2, 3, and 4). For the exclusion of old haemorrhage in hypointense areas on T2WI, we correlated the area with other sequence images. In addition, arterial rim enhancement persisting throughout portal venous and 3-min delayed phases was not regarded as capsule appearance. We evaluated dynamic enhancement patterns in the solid portions of tumours except for areas of haemorrhage and necrosis. A type I enhancement pattern was defined for a tumour showing arterial phase hyper-enhancement and washout appearance on portal venous or delayed phases. A type II enhancement pattern was defined for a tumour showing progressive enhancement or an unclassifiable enhancement pattern. The enhancement pattern referred to as "washout" was defined for lesions showing temporal reduction in enhancement relative to the liver from an earlier to a later phase resulting in portal venous phase or delayed phase hypo-enhancement [29]. Progressive enhancement was defined as persistent or gradual enhancement of a tumour on portal venous and 3-min delayed phase images compared with arterial phase images. Tumours with combined type I and type II enhancement patterns were regarded as having a type II enhancement pattern.

Statistical analysis

MR imaging features and levels of AFP and PIVKA-II were analyzed for comparison between the cholangio-combined and HCC groups using Wilcoxon rank-sum and Pearson chi-square tests. To ascertain the values of tumour markers and parameters for differentiating between the two groups, we used univariate logistic regression. Each logistic regression model provides *P* values and 95 % CI for odds ratios (OR).

For explicit identification of high-risk factors in the cholangio-combined group, a CTA was performed. The prediction model is obtained through a process described as follows. First, a single variable is found which splits the data into two subsets and which also minimizes impurities across the two subsets. In CTA, a set is pure if all the data in the set have a common outcome variable class level. The data are separated, and the process is then applied recursively to each derived subset. This recursive partitioning continues until the subsets reach a minimum size or no further improvement is expected. The partitioning can thus be represented graphically as a decision tree. After verification of the prediction tree model based on fivefold cross-validation (CV), we present a final model in which all the data is incorporated. We calculate sensitivity, specificity, positive predictive value (PPV) and negative predictive value (NPV), and diagnostic accuracy to evaluate our developed model [25].

Interobserver agreement regarding the MR imaging features of the lesions was evaluated by kappa (κ) statistics. A kappa value less than 0.20 indicated poor agreement; 0.21–0.40, fair agreement; 0.41–0.60, moderate agreement; 0.61–0.80, good agreement; and greater than 0.81, excellent agreement. Classification tree analysis was performed using the package "rpart" in R version 3.0.2 (Vienna, Austria; http://www.R-project.org/). All other statistical analysis was performed using SAS version 9.4 software (SAS Institute, Inc., Cary, NC, USA). All *P* values were two-sided, and $P < 0.05$ was considered statistically significant.

Table 3 Assessed MR imaging features and their definitions according to the favoured tumour group

Parameters	Definition	Favoured tumour group
Shape	Globular	HCC
	Non-globular	Cholangio-combined
Liver surface retraction	Liver border retraction periphery to tumour	Cholangio-combined
Biliary dilatation	Biliary obstruction disproportionate to that expected based on size of mass	Cholangio-combined
Intralesional fat (Fig. 3a, b)	Signal loss on out-of-phase compared to in-phase gradient echo images and its degree of signal low is greater than that of liver	HCC
Hyperintense area on T1WI	Area with signal intensity higher than that of the liver parenchyma, suggesting hemorrhagic foci	HCC
Hypointense area on T2WI	Area with signal intensity lower than that of the liver parenchyma, suggesting fibrosis	Cholangio-combined
Aggregated tiny hyperintense foci on T2WI (Fig. 2b)	Clustered tiny necrosis or cystic change	HCC
Arterial rim enhancement	Peripheral rim enhancement with central hypovascular area on arterial phase	Cholangio-combined
Capsule appearance	Peripheral rim of smooth hyper-enhancement in the portal venous phase or delayed phase that is unequivocally thicker or more conspicuous than the rim's surrounding background nodules	HCC
Target sign on DWI (b = 800) (Fig. 4c)	A central hypointense area and a peripheral hyperintense rim	Cholangio-combined
Target sign on 10-/20-min HBPI (Fig. 4d)	A central enhancement less than surrounding liver parenchyma and a peripheral hypointense rim	Cholangio-combined
Hyperintense area on 20-min HBPI	Area with signal intensity similar to or higher than that of the liver parenchyma	HCC
Dynamic enhancement pattern		
Type 1	Arterial phase hyper-enhancement with portal venous or delayed phase washout appearance	HCC
Type 2	Progressive enhancement or unclassifiable enhancement pattern	Cholangio-combined

T1WI T1-weighted images, *T2WI* T2-weighted images, *E* enhancement, *DWI* diffusion-weighted images, *HBPI* hepatobiliary phase images

Results

The levels of AFP and PIVKA-II were significantly different between the cholangio-combined group (mean, 9.46 ng/mL, 28.08 mAU/mL, respectively) and HCC group (mean, 490.8 ng/mL, 759.3 mAU/mL, respectively; $P = 0.0109$) (Table 1). However, the levels of AFP and PIVKA-II were elevated in 17 (26.6 %) and 5 (7.8 %) tumours, respectively, in the cholangio-combined group.

The MR imaging features for both groups are summarized in Table 4. Although there were significant differences between the two groups for all assessed parameters on MRI, most parameters were not perfect predictors for differentiating between the cholangio-combined and HCC groups. Intralesional fat was the only parameter shown exclusively in the HCC group, occurring in 24 (26.4 %) tumours. A type I enhancement pattern, which is considered typical of HCC, was shown in 12 (18.8 %) tumours of the cholangio-combined group, whereas 19 (20.9 %) tumours in the HCC group showed type II enhancement patterns (Figs. 2 and 3). Most of the assessed parameters on MRI showed good or excellent interobserver agreement, but interobserver agreement for enhancement pattern and the presence of fibrosis on T2WI was fair ($\kappa = 0.599$) and poor ($\kappa = 0.271$), respectively (Table 4). The OR of each imaging parameter for the differentiation of the two groups is also summarized in Table 4. Arterial rim enhancement, at 18.585, showed the highest OR for differentiating the cholangio-combined group from the HCC group.

In the CTA prediction model, arterial rim enhancement was the first splitting predictor for assessing the probability of a tumour being classified in the cholangio-combined group (Figs. 4 and 5). For tumours with arterial rim enhancement, the following predictors were no intralesional fat, non-globular shape of the tumour, target sign on DWI, no elevation of AFP level, and no hyperintensity on T1WI (Fig. 3). Of 43 tumours with arterial rim enhancement, no intralesional fat, and non-globular shape, 41 (95.3 %) were either IMCC ($n = 29$) or CHCs ($n = 12$). For tumours with no arterial rim enhancement, the following predictors were capsule appearance, elevated AFP level, no target sign on DWI, no liver surface retraction, elevated PIVKA-II level, and no biliary dilatation. The classification tree model established in this study has sensitivity of 84.4 %, specificity of 97.8 %, PPV of 96.4 %, NPV of 89.9 % and diagnostic accuracy of 92.3 % for discriminating the cholangio-combined group from the HCC group. In the HCC group, only two (3.2 %) tumours were classified in a high probability of cholangio-combined subgroup.

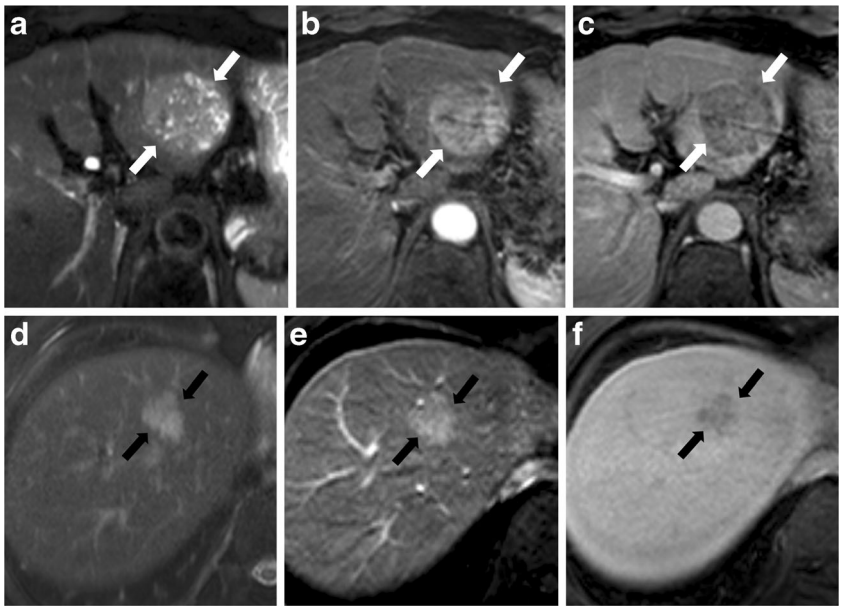

Fig. 2 Hepatocellular carcinoma (HCC, *top*, **a**–**c**) in left lateral liver with elevated PIVKA-II and combined hepatocellular-cholangiocarcinoma with HCC predominant type and normal tumour markers (CHC, *bottom*, **d**–**f**) in segment IV. HCC (*white arrows*) shows globular shape, aggregated tiny hyperintense foci on T2-weighted image (**a**) and type I enhancement pattern (arterial hyper-enhancement [**b**] and washout appearance on portal venous phase image [**c**]). CHC (*black arrows*) shows non-globular shape on T2-weighted image (d) and type I enhancement pattern on arterial (**e**) and 3-min delayed phase (**f**) images

Discussion

In this study, MR imaging features that had been evaluated for investigation of IMCC, CHC, and HCC in previous studies and tumour markers for HCC were significantly different between the IMCC and CHC group and the HCC group, although none but intralesional fat was a perfect predictor for the differentiation of IMCCs and CHCs from HCCs. Therefore, we sought to identify valuable combinations of predictors for differentiating IMCCs and CHCs from HCCs using a particular statistical methodology: CTA. We were able to establish a predictive algorithm with sensitivity of 84.4 %, specificity of 97.8 %, and diagnostic accuracy of 92.3 % for discriminating IMCCs and CHCs from HCCs.

CTA is a non-linear, non-parametric alternative to linear models for classification problems, in which classification trees are built for predicting class labels of outcome variables. In these tree structures, each interior node corresponds to one of the predictor variables. Leaves represent class labels of the outcome variable, and branches represent combinations of

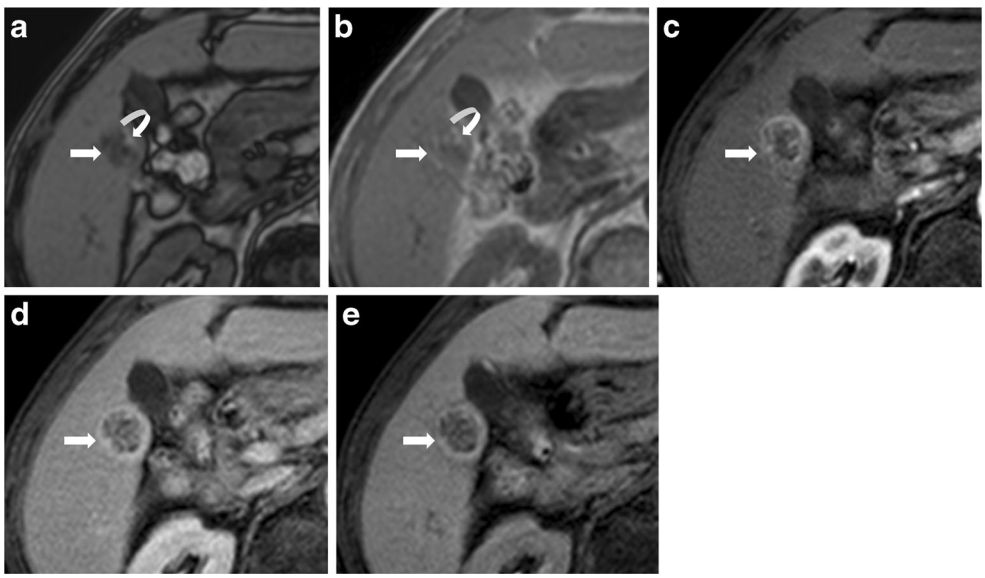

Fig. 3 A 57-year-old man with hepatocellular carcinoma in right lobe and normal tumour markers. The tumour (*arrows*) shows signal loss on out-of-phase imaging (**a**) compared with signal intensity on in-phase imaging (**b**), suggesting intralesional fat. Persistent hyperintense area (*curved arrows*) in the images is suggestive of hemorrhagic foci. Although the tumour shows arterial rim enhancement (**c**) and type II enhancement pattern on 3-min delayed-phase image (**d**), additional findings suggest HCC as globular shape, hyperintense area on T1-weighted image, intralesional fat, and hyperintensity on 20-min hepatobiliary phase image (**e**)

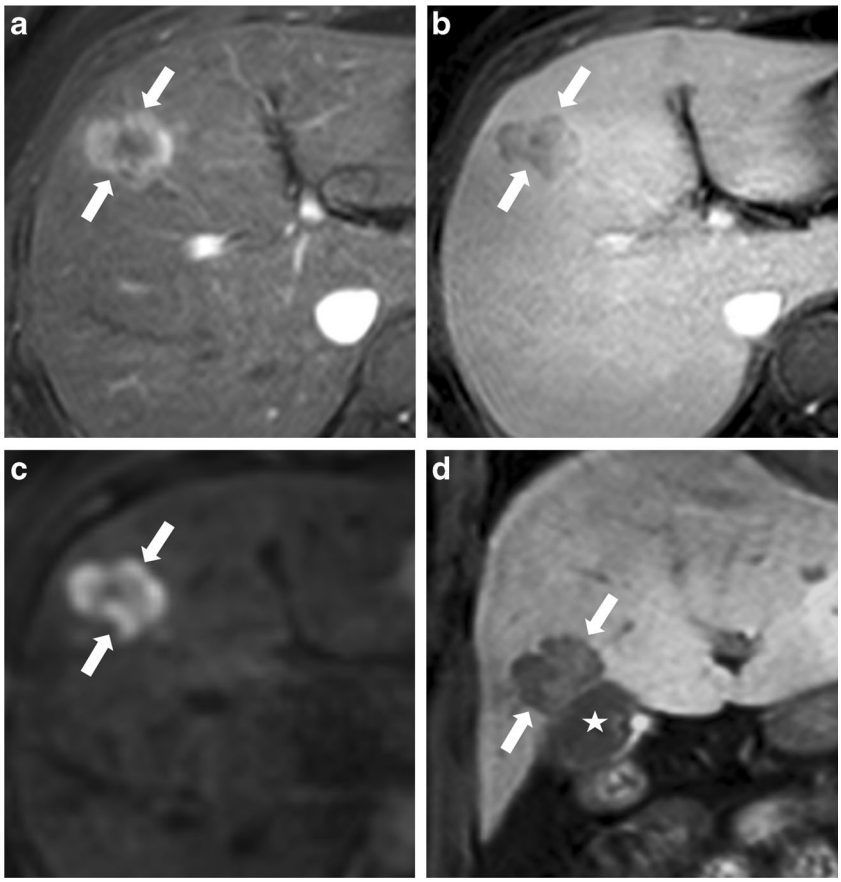

Fig. 4 A 63-year-old man with cholangiocarcinoma in segment IV and normal tumour markers. The tumour (*arrows*) shows non-globular shape, arterial rim enhancement and type II enhancement pattern on arterial (**a**) and 3-min delayed phase images (**b**). Target sign on DWI (b = 800 s/mm^2) (**c**) and 10-min hepatobiliary phase image (**d**) are also identified. *Asterisk* (*) indicates gallbladder

features that lead to those class labels. CTA offers a means for simple and explicit interpretation of results and judgment processes. In general, because it provides dichotomous cut points of predictor variables, CTA can provide class labels for outcome variables that are routinely required in clinical assessments. It also facilitates the identification and interpretation of complex interactions, whereas other multivariate analysis methods can handle only those interactions predetermined by the analyst. Several similar models have been revealed to be efficient tools for discriminating benign from malignant tumours or for identifying groups at high risk of a disease [30–32].

In this study, the typical enhancement pattern of HCC was not used as a predictor in CTA for assessing the probability of a tumour belonging to the cholangio-combined group. Although the typical HCC enhancement pattern is a valuable diagnostic criterion according to AASLD guidelines [6], atypical enhancements patterns on gadoxetic acid-enhanced MRI have been reported in 17.7–28.3 % of cases in previous studies [20, 21]. In the present study, 19 (20.9 %) HCCs showed atypical enhancement patterns. Differentiation of IMCCs and CHCs from atypical HCCs, therefore, can be challenging. The target sign on DWI was reported as a valuable imaging feature for distinguishing IMCCs from HCCs in a previous study [19], and it was used as a predictor for assessing the probability of classifying a tumour in the cholangio-combined group on CTA. In the CTA analysis of our study, 89 (97.8 %) tumours in the HCC group were classified as having a high probability for HCC, regardless of the tumour enhancement pattern.

In the present study, arterial rim enhancement, which showed the highest OR of 18.585 for differentiation between the cholangio-combined and HCC groups, was the first splitting predictor for assessing the probability of a tumour being classified as cholangio-combined on CTA. In a previous study by Jeong et al. [33], arterial rim enhancement was observed in 84–89 % of IMCCs, and was attributed to a greater density of viable tumour cells in the periphery with central fibrous stoma. Hwang et al. [34] reported that all 20 IMCCs and CHCs in their study showed strong or weak arterial rim enhancement. In addition, although 11 (12.1 %) tumours in the HCC group also showed arterial rim enhancement, nine (81.8 %) of those 11 were correctly classified as having high probability for HCC based on the presence of intralesional fat, globular shape, absence of target sign on DWI, elevation of AFP level, and presence of hyperintensity on T1WI. Therefore, when arterial rim enhancement is observed in a tumour in patients with CLD, the first differential diagnosis considered should be IMCC or CHC, although it is necessary to identify additional findings suggestive of HCC, as

Table 4 Qualitative and logistic regression analyses

Parameters	Cholangio-combined group	HCC group	*P* value*	*P* value†	Odds ratio	95 % CI	κ value
AFP elevation	17 (26.6)	51 (56.0)	0.0003	0.0004	0.284	0.142–0.567	NA
PIVKA-II elevation	5 (7.8)	45 (49.5)	<0.0001	<0.0001	0.087	0.032–0.236	NA
Globular shape vs.	10 (15.6)	49 (53.9)	<0.0001	<0.0001	0.159	0.072–0.35	0.735
Non-globular shape	54 (84.4)	42 (46.1)					
Liver surface retraction	16 (25)	5 (5.5)	0.0005	0.0013	5.733	1.978–16.623	0.803
Biliary dilatation	17 (26.6)	3 (3.3)	<0.0001	0.0003	10.608	2.957–38.051	0.670
Intralesional fat	0 (0)	24 (26.4)	<0.0001	NA	NA	NA	0.952
Hyperintensity on T1WI	2 (3.1)	18 (19.8)	0.0023	0.0079	0.131	0.029–0.586	0.943
Fibrosis on T2WI	15 (23.4)	8 (8.8)	0.0116	0.0146	3.176	1.256–8.033	0.271
Aggregated tiny hyperintense foci on T2WI	5 (7.8)	22 (24.2)	0.0082	0.0118	0.266	0.095–0.746	0.770
Arterial rim enhancement	46 (71.9)	11 (12.1)	<0.0001	<0.0001	18.585	8.078–42.756	0.860
Capsule appearance	2 (3.1)	38 (41.8)	<0.0001	0.0013	5.733	1.978–16.623	0.736
Target sign on DWI	31 (48.4)	9 (9.9)	<0.0001	<0.0001	8.559	3.677–19.925	0.854
Target sign on HBPI	39 (60.9)	12 (13.2)	<0.0001	<0.0001	10.27	4.670–22.583	0.701
Hyperintensity on HBPI	1 (1.6)	14 (15.4)	0.0042	0.0201	0.087	0.011–0.682	0.780
Type II enhancement vs.	52 (81.2)	19 (20.9)	<0.0001	<0.0001	16.421	7.335–36.763	0.599
Type I enhancement	12 (18.8)	72 (79.1)					

Note: Data are number of lesions. Numbers in parentheses are percentages. * *P* values and †*P* values were acquired using Pearson chi-square test and logistic regression model, respectively. *CI* confidence interval, *NA* not applicable (no cholangio-combined group showed intralesional fat on MRI), *T1WI* T1-weighted images, *T2WI* T2-weighted images, *DWI* diffusion-weighted images, *HBPI* hepatobiliary-phase images

mentioned previously. In recent years, arterial rim enhancement in HCCs has been considered a predictor of rapid progression, early recurrence, poor cellular differentiation, and worse tumour prognosis [17, 35, 36]. Therefore, surgical resection may be preferred over other treatment modalities, including TACE and RFA, for treatment of tumours with arterial rim enhancement in patients with CLD, although larger, more sophisticated studies would be needed.

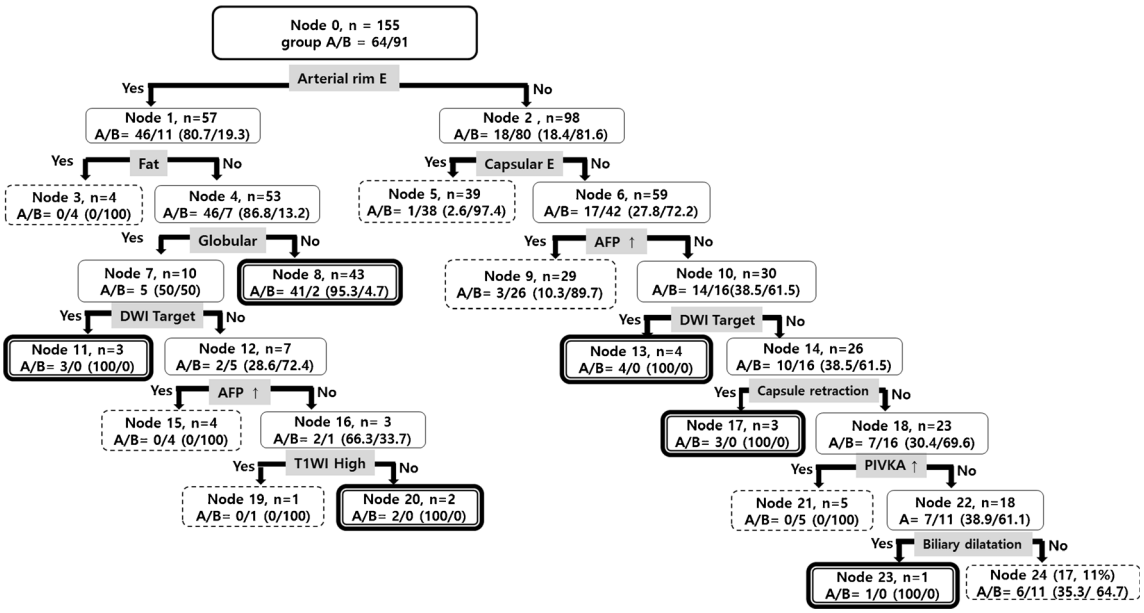

Fig. 5 Subgroups of the tumours identified through classification tree analysis and their risk of development for each group. Data are number of lesions. Numbers in parentheses are percentages. Group A = cholangio-combined group; Group B = hepatocellular carcinoma group. Boxes with *bold double-line* depict the subgroup of tumours with high probability of classification in the cholangio-combined group. Boxes with *dotted line* depict the subgroup of tumours with high probability of classification in the hepatocellular carcinoma group. *E* enhancement

In this study, none of the tumours in the cholangio-combined group showed intralesional fat. The presence of intralesional fat has been considered an ancillary feature that favours the diagnosis of HCC and a marker of carcinogenesis from dysplasia to HCC on CT or MRI [29, 37, 38]. This feature is attributable to a decrease in intratumoral arteries without alteration of intratumoral portal tracts [39]. Aasayama et al. reported the absence of fat as a key characteristic finding for IMCC, which may help its differentiation from poorly differentiated HCC [40].

This study has several limitations. First, selection bias may exist because of the retrospective study design, which included only patients with IMCC, CHC, or HCC who had undergone gadoxetic acid-enhanced MRI and hepatic surgery. Second, also because of the retrospective nature of the study, an exact correlation between the radiologic features and overall pathological composition was not performed. Third, as tumours included in this study met the Milan criteria, they were less than 5 cm in diameter. Therefore, the question remains whether our results would be useful in differentiating cholangio-combined from HCC groups for tumours greater than 5.0 cm in diameter. Fourth, the diagnostic performance of the CTA model in this study may be overestimated, as the performance results were obtained in the same study population as that for which the CTA model was developed. Therefore, validation of the model in a different study population or internal cross-validation would be needed to demonstrate whether the CTA model can be generalized to other population. In the present study, the performance of our CTA model was assessed based on internal validation (i.e., fivefold CV), and therefore our model may be over-fitted.

In conclusion, we established a simple classification tree model for differentiating IMCCs and CHCs from HCCs in primary liver cancers among a group of high-risk CLD patients. This classification tree model may be useful for guiding the diagnosis of primary liver cancers in patients with CLD.

Acknowledgments The scientific guarantor of this publication is J.M. Jang. The authors of this manuscript declare no relationships with any companies whose products or services may be related to the subject matter of the article. The authors state that this work has not received any funding. One of the authors, J. Kim, has significant statistical expertise.. Institutional Review Board approval was obtained. Written informed consent was waived by the Institutional Review Board. Methodology: retrospective, diagnostic or prognostic study, performed at one institution.

References

1. Sorensen HT, Friis S, Olsen JH et al (1998) Risk of liver and other types of cancer in patients with cirrhosis: a nationwide cohort study in Denmark. Hepatology 28:921–925
2. Shaib YH, El-Serag HB, Davila JA, Morgan R, McGlynn KA (2005) Risk factors of intrahepatic cholangiocarcinoma in the United States: a case-control study. Gastroenterology 128:620–626
3. Yamamoto S, Kubo S, Hai S et al (2004) Hepatitis C virus infection as a likely etiology of intrahepatic cholangiocarcinoma. Cancer Sci 95:592–595
4. Jarnagin WR, Weber S, Tickoo SK et al (2002) Combined hepatocellular and cholangiocarcinoma: demographic, clinical, and prognostic factors. Cancer 94:2040–2046
5. Chantajitr S, Wilasrusmee C, Lertsitichai P, Phromsopha N (2006) Combined hepatocellular and cholangiocarcinoma: clinical features and prognostic study in a Thai population. J Hepatobiliary Pancreat Surg 13:537–542
6. Bruix J, Sherman M, American Association for the Study of Liver D (2011) Management of hepatocellular carcinoma: an update. Hepatology 53:1020–1022
7. Lieser MJ, Barry MK, Rowland C, Ilstrup DM, Nagorney DM (1998) Surgical management of intrahepatic cholangiocarcinoma: a 31-year experience. J Hepatobiliary Pancreat Surg 5:41–47
8. Valverde A, Bonhomme N, Farges O, Sauvanet A, Flejou JF, Belghiti J (1999) Resection of intrahepatic cholangiocarcinoma: a Western experience. J Hepatobiliary Pancreat Surg 6:122–127
9. Yin X, Zhang BH, Qiu SJ et al (2012) Combined hepatocellular carcinoma and cholangiocarcinoma: clinical features, treatment modalities, and prognosis. Ann Surg Oncol 19:2869–2876
10. Sapisochin G, Fidelman N, Roberts JP, Yao FY (2011) Mixed hepatocellular cholangiocarcinoma and intrahepatic cholangiocarcinoma in patients undergoing transplantation for hepatocellular carcinoma. Liver Transpl 17:934–942
11. Lee WS, Lee KW, Heo JS et al (2006) Comparison of combined hepatocellular and cholangiocarcinoma with hepatocellular carcinoma and intrahepatic cholangiocarcinoma. Surg Today 36:892–897
12. Kadoya M, Matsui O, Takashima T, Nonomura A (1992) Hepatocellular carcinoma: correlation of MR imaging and histopathologic findings. Radiology 183:819–825
13. Maetani Y, Itoh K, Watanabe C et al (2001) MR imaging of intrahepatic cholangiocarcinoma with pathologic correlation. AJR Am J Roentgenol 176:1499–1507
14. Chong YS, Kim YK, Lee MW et al (2012) Differentiating mass-forming intrahepatic cholangiocarcinoma from atypical hepatocellular carcinoma using gadoxetic acid-enhanced MRI. Clin Radiol 67:766–773
15. Burns PN, Wilson SR (2007) Focal liver masses: enhancement patterns on contrast-enhanced images—concordance of US scans with CT scans and MR images. Radiology 242:162–174
16. Rimola J, Forner A, Reig M et al (2009) Cholangiocarcinoma in cirrhosis: absence of contrast washout in delayed phases by magnetic resonance imaging avoids misdiagnosis of hepatocellular carcinoma. Hepatology 50:791–798
17. Kawamura Y, Ikeda K, Hirakawa M et al (2010) New classification of dynamic computed tomography images predictive of malignant characteristics of hepatocellular carcinoma. Hepatol Res 40:1006–1014
18. Kang Y, Lee JM, Kim SH, Han JK, Choi BI (2012) Intrahepatic mass-forming cholangiocarcinoma: enhancement patterns on gadoxetic acid-enhanced MR images. Radiology 264:751–760
19. Park HJ, Kim YK, Park MJ, Lee WJ (2013) Small intrahepatic mass-forming cholangiocarcinoma: target sign on diffusion-weighted imaging for differentiation from hepatocellular carcinoma. Abdom Imaging 38:793–801
20. Choi YS, Rhee H, Choi JY et al (2013) Histological characteristics of small hepatocellular carcinomas showing atypical enhancement patterns on gadoxetic acid-enhanced MR imaging. J Magn Reson Imaging 37:1384–1391
21. Choi JW, Lee JM, Kim SJ et al (2013) Hepatocellular carcinoma: imaging patterns on gadoxetic acid-enhanced MR Images and their value as an imaging biomarker. Radiology 267:776–786
22. Shetty AS, Fowler KJ, Brunt EM, Agarwal S, Narra VR, Menias CO (2014) Combined hepatocellular-cholangiocarcinoma: what the

radiologist needs to know about biphenotypic liver carcinoma. Abdom Imaging 39:310–322
23. Silva MA, Hegab B, Hyde C, Guo B, Buckels JA, Mirza DF (2008) Needle track seeding following biopsy of liver lesions in the diagnosis of hepatocellular cancer: a systematic review and meta-analysis. Gut 57:1592–1596
24. Khan SA, Davidson BR, Goldin R et al (2002) Guidelines for the diagnosis and treatment of cholangiocarcinoma: consensus document. Gut 51(Suppl 6):VI1–VI9
25. Leo Breiman , Jerome Friedman, Charles J. Stone and R.A. Olshen (1984) Classification and Regression Trees. Chapman and Hall/CRC
26. Befeler AS, Hayashi PH, Di Bisceglie AM (2005) Liver transplantation for hepatocellular carcinoma. Gastroenterology 128:1752–1764
27. Marti-Bonmati L, Talens A, del Olmo J et al (1993) Chronic hepatitis and cirrhosis: evaluation by means of MR imaging with histologic correlation. Radiology 188:37–43
28. Koh J, Chung YE, Nahm JH et al (2015) Intrahepatic mass-forming cholangiocarcinoma: prognostic value of preoperative gadoxetic acid-enhanced MRI. Eur Radiol. doi:10.1007/s00330-015-3846-5
29. American College of Radiology (2013) Liver Imaging Reporting and Data System version 2013.1. http://www.acr.org/Quality-Safety/Resources/LIRADS/. Accessed Jan 2013
30. El Malki HO, El Mejdoubi Y, Souadka A et al (2010) Predictive model of biliocystic communication in liver hydatid cysts using classification and regression tree analysis. BMC Surg 10:16
31. Thomassin-Naggara I, Toussaint I, Perrot N et al (2011) Characterization of complex adnexal masses: value of adding perfusion- and diffusion-weighted MR imaging to conventional MR imaging. Radiology 258:793–803
32. Nunes LW, Schnall MD, Orel SG (2001) Update of breast MR imaging architectural interpretation model. Radiology 219:484–494
33. Jeong HT, Kim MJ, Chung YE, Choi JY, Park YN, Kim KW (2013) Gadoxetate disodium-enhanced MRI of mass-forming intrahepatic cholangiocarcinomas: imaging-histologic correlation. AJR Am J Roentgenol 201:W603–W611
34. Hwang J, Kim YK, Park MJ et al (2012) Differentiating combined hepatocellular and cholangiocarcinoma from mass-forming intrahepatic cholangiocarcinoma using gadoxetic acid-enhanced MRI. J Magn Reson Imaging 36:881–889
35. Kierans AS, Leonardou P, Hayashi P et al (2010) MRI findings of rapidly progressive hepatocellular carcinoma. Magn Reson Imaging 28:790–796
36. An C, Kim DW, Park YN, Chung YE, Rhee H, Kim MJ (2015) Single Hepatocellular Carcinoma: Preoperative MR Imaging to Predict Early Recurrence after Curative Resection. Radiology 142394
37. Yu JS, Chung JJ, Kim JH, Kim KW (2007) Fat-containing nodules in the cirrhotic liver: chemical shift MRI features and clinical implications. AJR Am J Roentgenol 188:1009–1016
38. Martin J, Sentis M, Zidan A et al (1995) Fatty metamorphosis of hepatocellular carcinoma: detection with chemical shift gradient-echo MR imaging. Radiology 195:125–130
39. Kutami R, Nakashima Y, Nakashima O, Shiota K, Kojiro M (2000) Pathomorphologic study on the mechanism of fatty change in small hepatocellular carcinoma of humans. J Hepatol 33:282–289
40. Asayama Y, Nishie A, Ishigami K et al (2015) Distinguishing intrahepatic cholangiocarcinoma from poorly differentiated hepatocellular carcinoma using precontrast and gadoxetic acid-enhanced MRI. Diagn Interv Radiol 21:96–104